Martin WAGNER[1*], Mohaned ALALUSS[1], Robin KURTH[1],
Robert TEHEL[1], Franz REUTHER[1], Steffen IHLENFELDT[1,2]

CHARACTERIZATION OF THE MACHINE BEHAVIOUR DURING HOLLOW EMBOSSING ROLLING OF METALLIC BIPOLAR HALF PLATES

The hollow embossing rolling of thin-walled high precision components like metallic bipolar half plates is characterized by narrow process windows. Here, the knowledge of interaction between forming machine, roll and process is crucial for the process stability and quality of formed bipolar half plates. In this paper, the elastic machine and forming roll behaviour as a major influence parameter is described and analysed on qualitative level and verified by simulation. This investigation involves a review regarding the process sequence, forces for the hollow embossing rolling of metallic bipolar half plates. By varying the load distributions, the elastic deformations of the forming machine and their forming roll are investigated and analysed regarding process influence and potential for process monitoring.

1. INTRODUCTION

Ongoing climate change and upheavals in energy and resources require a global move away from the use of finite fossil fuels towards environmentally friendly alternatives. In the field of energy supply and especially in the transport sector, electrification of the drive train is therefore increasingly taking place, combined with hydrogen as a carbon-free energy carrier [1]. Metallic bipolar plates as key components of hydrogen-powered fuel cells in electric drive systems are characterized as complex and thin-walled precision components [2]. An approach to manufacture these complex and thin-walled precision components is the use of forming processes like the hollow embossing [3] and high-pressure sheet forming [4], which are characterized as discontinuous processes in terms of material feed and press kinematics. While these manufacturing processes are known and the required machine technology are well established, they are limited regarding the accuracy, production rate, and profitability [5]. However, to meet the increasing demand for components in connection with the electric

drive type based on a hydrogen-powered fuel cell, high-rate production processes are necessary.

A promising forming technology is the hollow embossing rolling of complex and thin-walled precision components, which enables to increase the production rate significantly and to deliver high-quality components at the same time [2, 6]. In contrast to translational processes, the machine technology for the rolling of thin-walled precision components is not well established and little researched [7, 8]. In particular, the knowledge of interdependencies between the rolling process and forming machine is crucial for the rolling process of thin-walled components with demands on dimensional accuracy and shape precision. Considering very high quantities, a holistic investigation of the interdependencies between the forming machine and forming rolls is still missing.

Therefore, the aim of this scientific contribution is to describe and investigate the mentioned complex interactions during the hollow embossing rolling of metallic bipolar half plates (BP-HP) on qualitative level in Chapter 2 and verify them by simulative analysis in Chapter 3. Here, the focus is set on the simulative analysis of the elastic machine behaviour. Based on the results obtained the potential benefit regarding process influence and process monitoring are discussed. Moreover, the gained insights enable to optimize available forming machines and tools for manufacturing of thin-walled precision components like metallic BP-HP, which promises to increase the robustness of the forming process. To conclude the paper, a summary and outlook are given.

2. PROCESS CHARACTERISTIC OF HOLLOW EMBOSSING ROLLING

2.1. PROCESS SEQUENCE AND FORCES

Compared to established forming processes like hollow embossing [2] and hydro-forming, hollow embossing rolling involves forming of a metal sheet strip between two rotating forming rolls, as illustrated in Fig. 1.
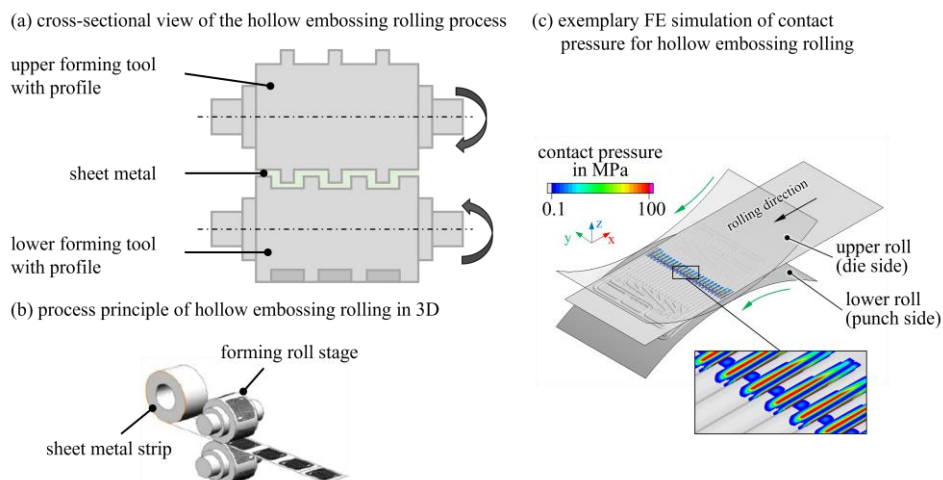

Fig. 1. Schematic representation of the hollow embossing rolling in (a) cross-sectional view adopted from [2] and in (b) a 3D view as well as (c) an exemplary FE analysis regarding the contact pressure distribution in the roll gap

Due to the continuous rotation of the forming rolls, the forming operation is comparable to an incremental forming behaviour. As shown in Fig. 1b, the interacting machine components during the forming operation can be characterized as the forming tools in form of rolls, where one forming roll is defined as a punch, the other as a die and two pairs of feeding rolls. Initially, a strip tension is built by using a feed rolling stage with the help of a braking torque for the subsequent forming operation. During this forming operation, the correspondingly structured areas meet each other, whereby the sheet metal strip is formed between the forming rolls. As a result of the roll rotation, there is a translational transport effect on the material to be formed. After the incremental forming phase, a third rolling stage follows, which ensures that the strip is safely guided away from the forming zone. A major problem in rolling thin channel structures is the thinning of the film in the forming zone [9, 10]. Furthermore deformation-induced axial and radial contractions result in wrinkles and minimal deviations from the nominal geometry. In addition, Bauer et al. [8] observed a global deformation of the BP-HP occurred due to spring back [11]. Moreover, the spring back during rolling of the BP-HP leads to shape deviations. This can lead to problems during joining, stacking and performance losses (due to the different surface pressure) of the BP-HP. In addition, preliminary work showed that a shape and dimension accuracy of less than 0.005 mm for the final BP-HP is required based on sheet metal strips with an initial thickness of 0.05 to 0.1 mm [5].

Regarding process forces and their magnitude, they are significantly lower than for the other processes considered due to the incremental forming character. In the FE analysis performed by Porstmann et al. [10] the maximum forming forces for hollow embossing amount to only 13 kN. As illustrated in Fig. 1c, the simulated contact pressure distribution in the sheet metal strip between upper and low forming roll reach the highest values (up to 100 MPa) in the lower edges of the BP-HP channel ground. Additionally, to the technological challenges, there are challenges on the machine side regarding concept development and monitoring due to the very high demands on dimensional and shape accuracy of the manufactured BP-HP. Especially, publications like the work of Tehel et al. [12] shows the great influence of the elastic machine behaviour and properties on the success of a resistant forming process and on the necessary technology parameters.

3. SIMULATIVE ANALYSIS OF THE ELASTIC MACHINE AND FORMING ROLL BEHAVIOUR

3.1. MODEL DESCRIPTION AND IMPLEMENTATION

To meet the very high requirements regarding the shape and dimension accuracy of the formed BP-HP, the knowledge of interdependencies between the forming machine, rolls and process is dispensable. In this paper, the simulative analysis using the finite-element method (FEM) through the software ANSYS® is a promising approach to investigate the influence of the acting forces and their variation regarding the magnitude and its location. As depicted in Fig. 2a, a machine concept for hollow embossing rolling of BP-HP is available at Fraunhofer IWU and is used for the simulative investigations.
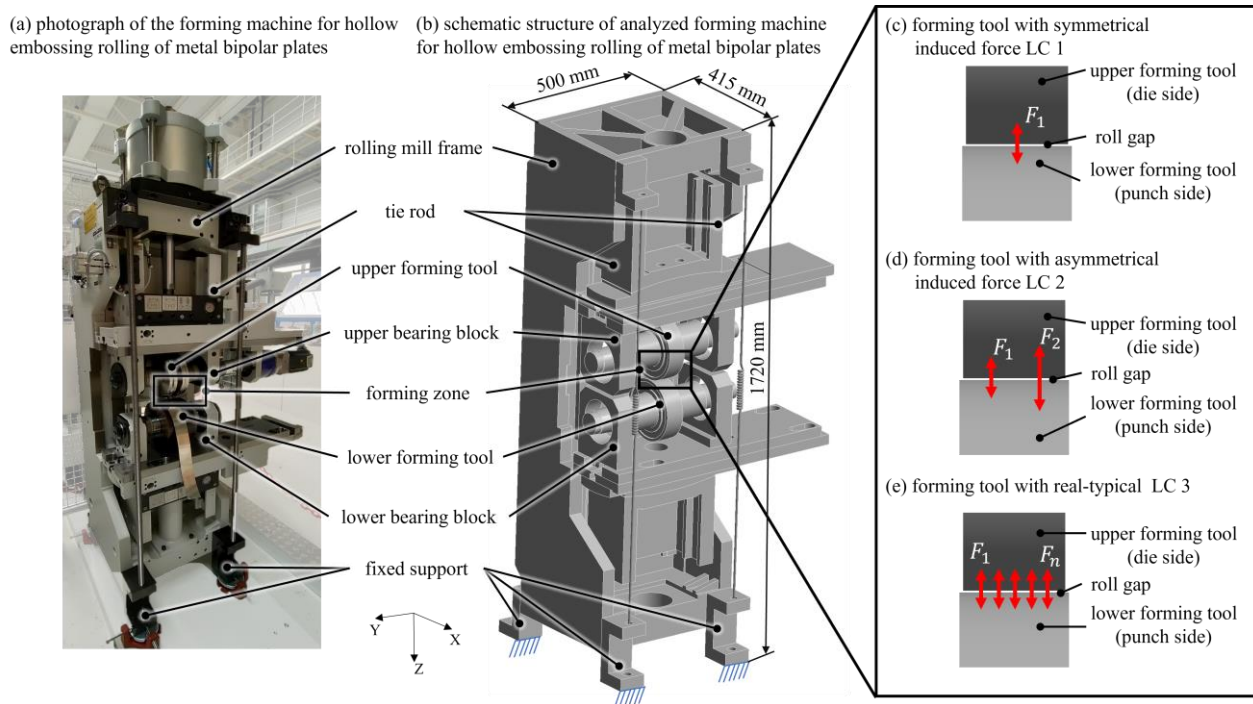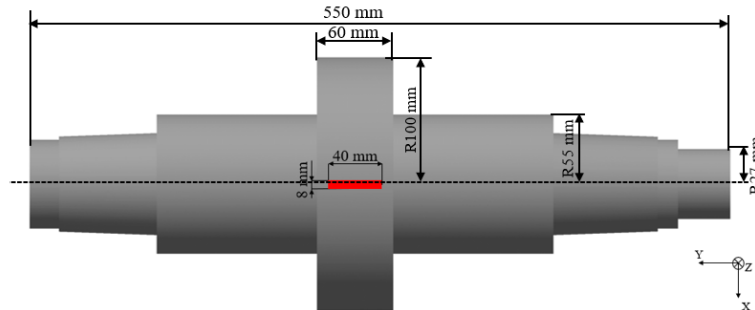
Fig. 2. Photograph of the analysed forming machine for hollow embossing rolling – (a) and CAD model – (b), defined LC – (c) to (e) for the simulative analysis

To acquire a detailed insight into the elastic behaviour of the forming machine and the forming tool in form of the forming rolls, static elasto-mechanical simulations of the forming machine and the rolls are performed. The general procedure for the FE analysis is structured in two single steps. While in the first step the entire forming machine is considered in the simulative investigations, the second step focuses on the forming rolls and the forming zone. In the simulative analysis three load cases (LC) are realized by varying the force application point, as illustrated in Fig. 2c to 2e. Thereby, LC 1 represents an ideally uniformly distributed force distribution in the roll gap, whereas LC 2 represents an asymmetrical load distribution with 50% load difference between the left and the right side of the forming rolls - e.g., due to an uneven sheet metal strip thickness or non-parallel forming rolls. Furthermore, LC 3 describes a real-typical load distribution in the roll gap resulting from the hollow embossing rolling process for BP-HP.

Based on preliminary works in form of forming simulations boundary conditions like the forming force magnitude and distribution are derived for the static elasto-mechanical simulations of the forming machine and the rolls. In this regard, the preliminary forming simulations assumed a metal sheet strip material of stainless steel 1.4404 with a thickness of 0.1 mm as well as sheet dimensions of 50 mm total width (for forming effective width of 40 mm) for a small forming roll and a total width of 210 mm (for forming effective width of 200 mm) for a large forming roll. By defining two force application areas in the simulation analysis, as depicted in Fig. 3, the influence of different BP-HP geometries and sizes are evaluated regarding the elastic machine and forming roll behaviour. For the small forming roll the force application area is characterized by a forming roll surface of 320 mm², where the forming takes place. Meanwhile, for the large forming roll a surface size of 1600 mm² has

been defined. Regarding the forming force magnitude, a value of 25 kN is set for the small forming roll, while for the large forming roll a value of 125 kN is defined.
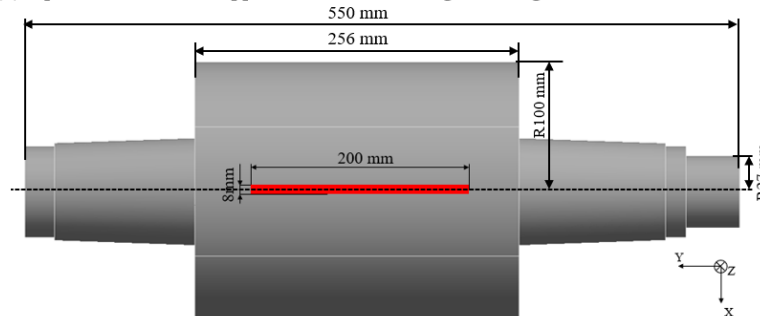

Fig. 3. Definition of force application area for (a) small forming tool and (b) large forming tool

    The area for the application of the forming force in Fig 3 is marked with a red square in the contact area of the forming rolls. In addition, forming simulations have shown, for this specific case, that the initial forming contact occurs 5° before reaching the forming roll axis plane. Regarding the boundary conditions of the FE model, a fixed support of the machine foundation is defined. For all machine components, especially the forming rolls structural steel with an elasticity modulus of 200000 MPa and Poisson's ratio of 0.3 is assumed. Due to the linear elastic simulation, the elastic behaviour of the forming roll is completely mapped over the two values. Also, it was presumed that the bearing of the forming rolls has the radial rolling bearing stiffness of 165000 N/mm specified by the bearing manufacturer. To ensure the required stiffness of the forming machine, the model consists of a C-frame with two tie rods. The required pretension of these tie rods is achieved with a preload force of 2.5 kN. To keep the calculation memory consumption of the FE analysis appropriate, the mesh size is demand driven. Here, the meshing is based on a mixed meshing with tetrahedra and hexahedra, with center nodes (quadratic attachment function). Thus, the contact areas of the forming zone including the forming rolls a finer mesh is applied whereas a relatively coarse mesh is suitable for most of the structure. For the overall model (forming machine and forming rolls) consisting of 1.2 million nodes, a calculation time of one hour results. Further on, the submodel of the forming rolls is meshed with the same parameters and consists of 3 million nodes, which results in a calculation time of 20 minutes due to the missing contacts compared to the overall model.

3.2. ELASTIC DISPLACEMENT OF THE MACHINE FRAME AND FORMING ROLL

The acting forming forces lead not only to elastic deformation of the machine frame and forming rolls but also to an elastic displacement of the machine frame respectively an elastic deflection of the forming rolls, as illustrated in Fig. 4. Here, for LC 1 to LC 3 at two force magnitudes (25 kN and 125 kN) the resulting elastic displacement distribution of the machine frame and the elastic deflection of the lower forming roll along the z-coordinate are displayed.

force	assembly	LC 1	LC 2	LC 3
25 kN	machine frame			
	lower roll deflection			
125 kN	machine frame			
	lower roll deflection			

0,55   0,28   -0,01   -0,25   -0,54   -0,80

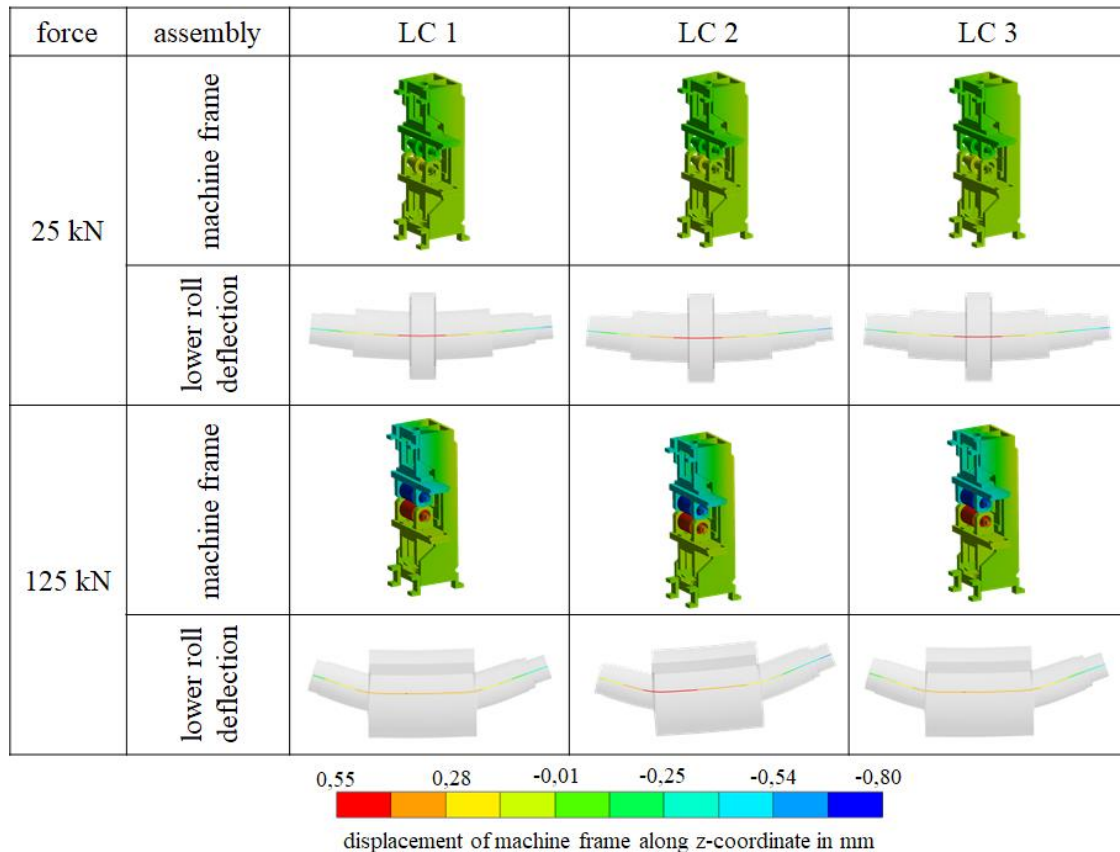displacement of machine frame along z-coordinate in mm

Fig. 4. Elastic deformation of the machine frame and exaggerated elastic deflection of the lower small as well as large forming roll (scale factor 550x)

While the elastic deformation of the machine frame is shown with a scale of 1, the elastic deflection of the lower forming rolls is exaggerated by a scale factor of 550 to visually present the results with a uniform scale. The direct comparison of the different LC 1 to LC 3 shows a little influence of the load cases on the elastic deformation of the machine frame. Likewise, the elastic deformation of the small forming roll with a force magnitude of 25 kN, is comparable in all load cases. Using a large forming roll in correspondence with a higher forming force of 125 kN, higher elastic displacement values regarding the machine frame as well as elastic deflection values in the lower roll can be observed. Compared to the small forming roll, a clear correlation between the load cases LC 1 to LC 3 and the resulting elastic deflection can be seen. For the asymmetrical LC 2, the maximum deflection value of 0.48 mm

can be detected, which almost coincides with the defined force application point. One major reason lies in the large forming area with a high force magnitude, which has a significantly higher impact on the elastic displacement behaviour compared to small forming roll. The maximum permissible shape and dimension deviation for the machine frame and rolls can be defined as a value of ±0.01 mm.

Figure 5a shows the elastic displacement distribution of the whole forming machine involving the small forming rolls for LC 1, while Fig. 5b to d depict the elastic displacement distribution in the forming zone of the lower forming roll in form of a false colour representation. Here, it can be stated that the simulated elastic displacement values for LC 2 and LC 3 regarding the forming machine frame are similar in general, as already shown in Fig. 4. For the forming machine frame elastic displacement along the z-coordinate values between -0.18 and 0.12 mm can be registered, as depicted in Fig. 5a.
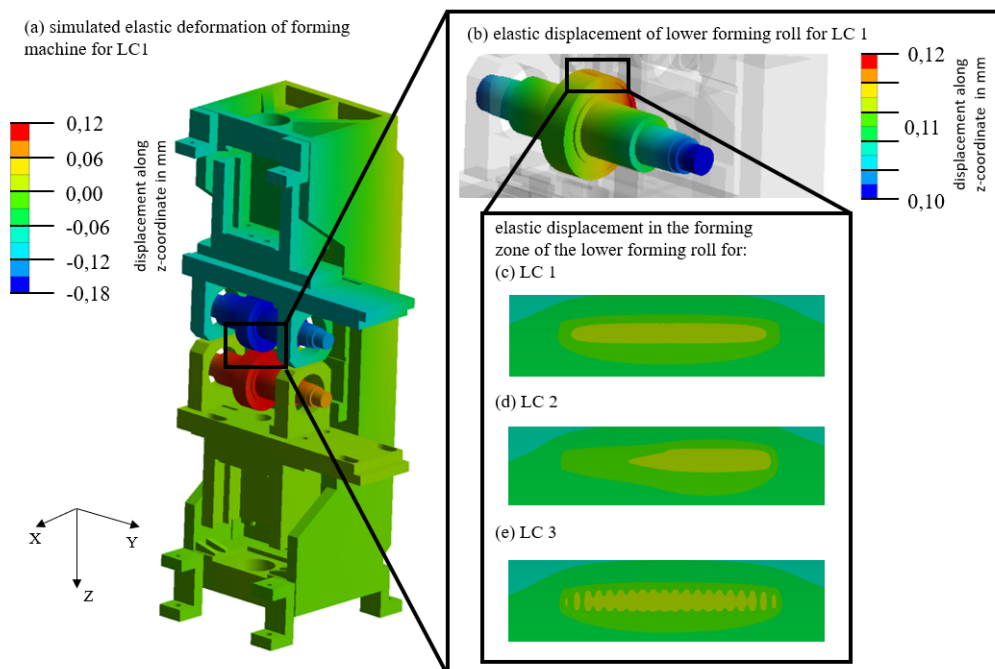

Fig. 5. (a) Simulated elastic displacement of the forming machine, (b) elastic deformation of the lower forming roll for (c) symmetrical load case LC 1, (d) asymmetrical load case LC 2 and (e) realistic load case LC 3

Compared to the analysed elastic machine frame behaviour, significant differences in the elastic displacement values at the forming zone depending on the applied LC for the lower small roll can be detected, as shown in Fig. 5c to 5e. By means of a false colour representation, different elastic displacement areas at the lower roll surface can be identified. As displayed in Fig. 5c, a uniform elastic displacement along the entire forming area could be determined simulatively due to a simplified symmetrical LC 1. The elastic displacement values lie in a range of 0.12 mm in the forming zone. For the asymmetrical LC 2, a clear separation between the force ranges is visible, which can be explained by the FE model structure including two zones with different forming forces. The elastic displacement values are in a range of 0.10 mm on the left-hand side and 0.12 mm on the right-hand, higher loaded side.

Regarding the real-typical LC 3, elastic displacement values of 0.10 mm in the less deformed forming areas can be observed, whereas in the interstices of the channel structures the elastic displacement distribution reaches values of about 0.12 mm.

Further on, the elastic deflection of the lower forming roll is used for a more detailed evaluation regarding the influence of the applied forming forces. Figure 6 shows the context between the resulting elastic deflection of the small as well as large lower forming roll under the defined LC 1 to LC 3 along the neutral axis over the entire lower forming roll width.
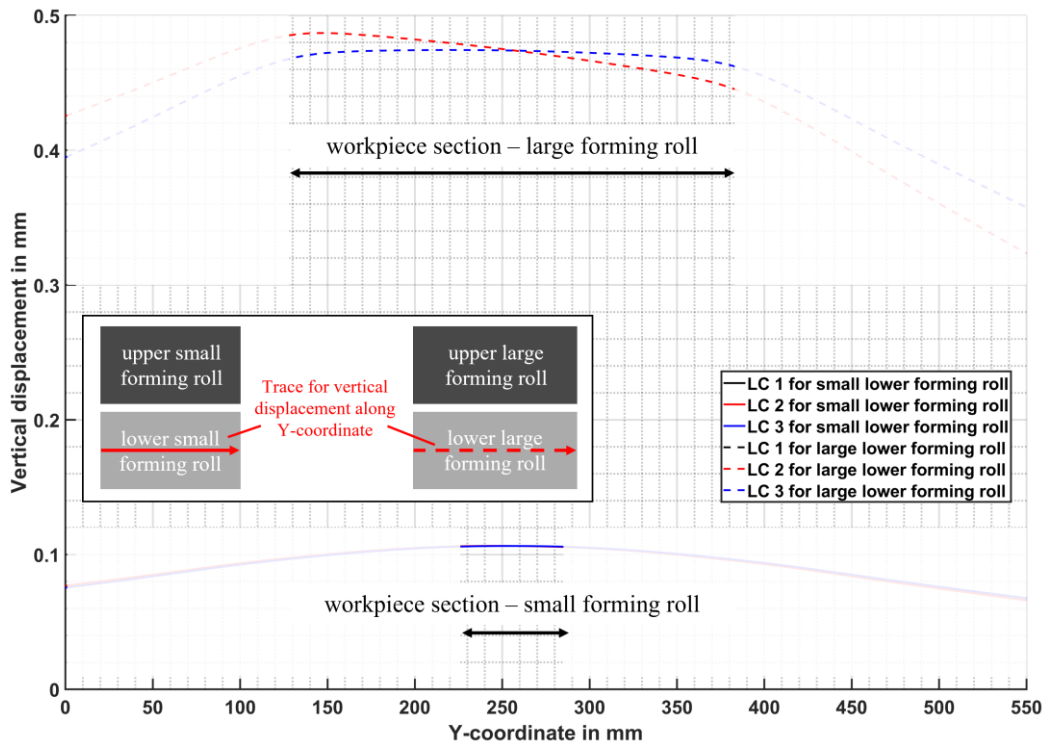

Fig. 6. Simulated displacement changes of lower forming roll along the neutral axis for LC 1 to LC 3

In comparison to the elastic displacement in the forming zone, the absolute elastic deflection values of the forming rolls are higher and reach values between 0.48 mm for the large rolls and 0.1 mm for the small rolls. Consequently, the relative change of about 0.08 mm for the large rolls and 0.02 mm for the small rolls can be derived.

As already mentioned, the elastic displacement for the LC 1 and LC 2 can be distinguished clearly well for the large forming roll. In contrast, the simulated displacement values for LC 1 and LC 3 hardly differ. The exact distribution of local forces, evoked through the channel structure of the BP-HP in LC 3, shows no significant effect on the behaviour of the elastic deflection behaviour of the forming rolls. With respect to LC 2 the results show for the right-hand side approximately 50% higher relative elastic displacement values then at the left-hand forming roll side due to the asymmetric character of the forming force application. For the small forming roll, the differences between the LC's are significantly less. As already mentioned above, the reason can be explained by the lower forming forces compared to the large rolls and the locally very limited forming area.

3.3. ELASTIC STRAIN BEHAVIOUR OF THE MACHINE FRAME AND FORMING ROLL

To analyse the elastic deformation behaviour of the forming machine frame and forming roll, a representation comparable to Fig 5 is used. Thereby, Fig. 7 shows the elastic strain distribution representing the elastic deformation behaviour of the forming machine and forming roll due changes in the acting forming forces. While Fig. 7a plots the uniform elastic strain behaviour of the machine frame for LC 1, Fig. 4b to 4e show the elastic strain values of the lower small forming roll for LC 1 to LC 3.
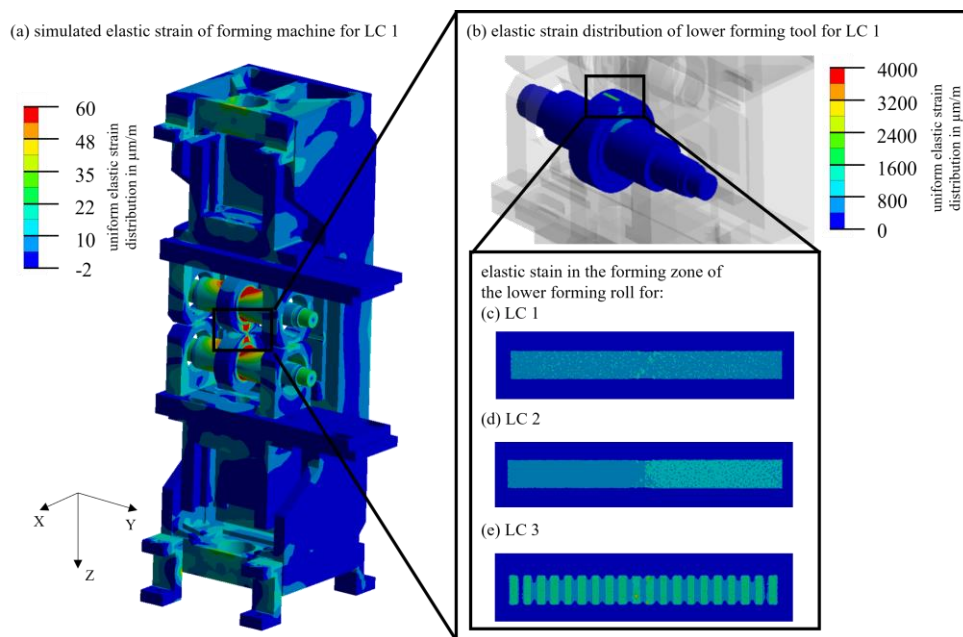

Fig. 7. (a) Simulated elastic strain of the forming machine, (b) elastic strain of the lower forming roll, (c) symmetrical load case LC 1, (d) asymmetrical load case LC 2 and (e) realistic load case LC 3

Like the elastic displacement behaviour of the machine frame the simulated elastic strain distribution of the machine frame shows a similar behaviour for all three LC's. Here, for all LC's elastic strain values between -2 and 60 µm/m can be registered, as depicted in Fig 4a. In comparison to the analysed elastic machine frame behaviour, significant differences in the elastic strain values depending on the specific LC for the lower small roll can be detected, as shown in Fig 7c to e. Further on, different elastic strain areas at the lower roll surface can be identified using a false colour representation. As it can be seen in Fig. 7a, a uniform elastic strain distribution along the entire forming area could be determined simulatively due to a simplified symmetrical LC 1. The elastic strain reaches a value of 80 µm/m in the forming zone. For the asymmetrical LC 2, a clear separation between the applied force ranges is visible, which can be explained by the FE model structure including two zones with different forming forces. The elastic strain values are in range of 60 µm/m on the left-hand side and 90 µm/m on the right-hand, higher loaded side. Regarding the real-typical LC 3, elastic strain values of 50 µm/m in the less strained forming areas can be observed, whereas in the interstices of the channel structures of the BP-HP the elastic strain distribution reaches values of about 200 µm/m.

As already mentioned, the elastic strain distribution for the LC 1 to LC 3 can be distinguished clearly well. Moreover, the simulated strain values for LC1 and LC3 differ in the magnitude due to the different size of the force application areas. Also, the geometry of the BP-HP in form of the implemented channel structure in LC 3 shows a great influence on the force distribution and therefore the resulting elastic strain distribution, which reduce the force application area by half the size of the implemented force application area in LC 1. In addition, the peaks created by this channel structure, can be easily determined. The results of LC 2 show for the right-hand side 50% higher elastic strain values then at the left-hand forming tool side due to the asymmetric character of the process force application.
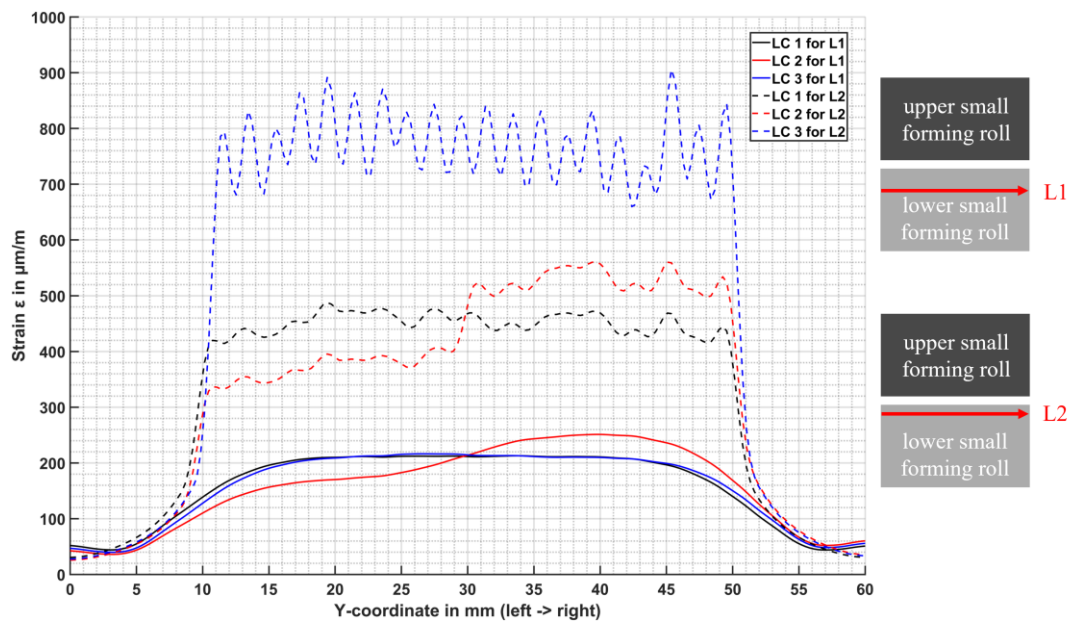

Fig. 8. Simulated elastic strain changes of lower forming roll along measurement line L1 (10 mm below lower small roll surface) and L2 (0.1 mm below lower small roll surface) for LC 1 to LC 3

Additionally, the relationship between the distance to the forming zone and the resulting strains is shown in Fig. 8. Two measuring lines L1 (10 mm below lower small roll surface) and L2 (0.1 mm below lower small roll surface) are defined for this purpose. For L2, the simulated results show two main differences to the results for L1. In general, the elastic strain values are clearly lower which is explainable by the distance to forming zone. Below L2 value of 10 mm, a distinction between the simulated strain values of LC 1 and LC 3 is possible. Furthermore, the elastic strain distribution shows a homogeneously distribution over the entire forming roll width, which can be assumed as the ideal condition for hollow embossing rolling.

4. SUMMARY AND FUTURE WORK

The proposed simulation model enables to describe and analyse the elastic behaviour of the forming machine and forming rolls during the hollow embossing rolling of metallic bipolar half plates. As the investigations in Section 3.2 and 3.3 have shown, the influence

of the elastic machine and forming roll properties in form of the elastic displacement and elastic strain distribution is significant for a successful hollow embossing process. Key conclusions can be summarized as follows:

- The elastic behaviour of the forming machine and forming rolls in form of elastic displacement and strain values are significant and measurable using measurement technology.
- The closer to the forming zone, the greater the values of the elastic displacement and strain values. Furthermore, asymmetric loads can be identified in the elastic displacement and strain distribution, especially in the forming rolls.
- A secure and sensitive inline measurement as close as possible to the forming zone is key to enable a high precision resolution of e.g., the force distribution in the roll gap. The major challenge lies in the resilient implementation of sensor technologies as close as possible to the forming zone without affecting the functionality or robustness of the forming machine and rolls.

In future work, the simulatively attained results need to be verified by experimental investigations. One interesting aspect is to investigate the dynamic behaviour of the forming machine resulting from the cutting operations, but also from the drives in all active roll, and their influence on the metallic BP-HP quality. Based on these investigations new sensor concepts considering the identified correlation and sensor integration strategies must be developed and experimentally evaluated.

Consequently, the obtained the simulation results can contribute to the primary goal of ensuring as well as increasing the process stability and the resulting component quality by modifying for instance the forming tools in relation to their zero geometry according to the identified elasticities of the forming machine and rolls.

REFERENCES

[1]   Federal Ministry of Education and Research, 2022, *National Hydrogen Strategy: Green Hydrogen as Energy source of the future, https://www.bmbf.de/bmbf/en/news/national-hydrogen-strategy.html*, Accessed on: 29 Dec. 2022.
[2]   PORSTMANN S., WANNEMACHER T., DROSSEL W.-G., 2020, *A Comprehensive Comparison of State-of-the-Art Manufacturing Methods for Fuel Cell Bipolar Plates Including Anticipated Future Industry Trends*, Journal of Manufacturing Processes, 60, 366–383.
[3]   LIU Y., HUA L., 2010, *Fabrication of Metallic Bipolar Plate for Proton Exchange Membrane Fuel Cells by Rubber Pad Forming*, J. Power Sources, 195, 3529–3535.
[4]   MOHAMMADTABAR N., BAKHSHI-JOOYBARI M., HOSSEINIPOUR S.J., GORJI A.H., 2016, *Feasibility Study of a Double-Step Hydroforming Process for Fabrication of Fuel Cell Bipolar Plates with Slotted Interdigitated Serpentine Flow Field*, Int. J. Adv. Manuf. Technol., 85, 765–777.
[5]   PORSTMANN S., PETERSEN A.C., WANNEMACHER T., 2019, *Analysis of Manufacturing Processes for Metallic and Composite Bipolar Plates*, (FC³) Fuel Cell Conference Chemnitz, 25–39.

[6] POLSTER S., PORSTMANN S., 2023, *FOSTA Projekt Bipolarplatten: Verfahrensvergleich zur Formgebung metallischer Bipolarplatten – Hohlprägen vs. Hohlprägewalzen*, https://hzwo.eu/project/fosta-bipolarplatten-praegen/, Accessed on: 05 June 2023.

[7] BAUER A., HÄRTEL S., AWISZUS B., 2019, *Manufacturing of Metallic Bipolar Plate Channels by Rolling*, J. Manuf. Mater. Process, 3, 48.

[8] PORSTMANN S., WANNEMACHER T., RICHTER T., 2019, *Overcoming the Challenges for a Mass Manufacturing Machine for the Assembly of PEMFC Stacks*, Machines, 7, 66.

[9] ZHANG P., PEREIRA M., ROLFE B., DANIEL W., WEISS M., 2017, *Deformation in Micro Roll Forming of Bipolar Plate*, J. Phys.: Conf. Ser. 896 012115.

[10] PORSTMANN S., POLSTER S., REUTHER F., MELZER S., NAGEL M., PSYK V., DIX M., 2022, *Objectives and Fields of Tension in the Comparison of Manufacturing Processes for Metallic Bipolar Plates*, (FC³) Fuel Cell Conference Chemnitz, 195–208.

[11] BUDDHIKA A., ZHANG P., PEREIRA M., WILKOSZ D., WEISS M., 2019, *Micro-Roll Forming of Stainless Steel Bipolar Plates for Fuel Cells*, International Journal of Hydrogen Energy, 44, 2861–3875.

[12] TEHEL R., PÄßLER T., MIHM M., 2019, *Modeling Elastic Behavior of Forming Machine Components to Reduce Tool Manufacturing Time*, Procedia Manufacturing, 27, 177–184.